

15. The low mass of the ^{11}B nucleus makes it the optimal ion for detection of cation-anion pairs in the catalyst bead. A sample of catalyst was mounted in a resin matrix and then microtomed to give a flat surface for the SIMS analysis. Figure 3 shows two beads, one of which displays a larger cross section than the other because it was machined to a different depth.
16. X.-D. Xiang *et al.*, *Science* **268**, 1738 (1995).
17. This work partially funded from NSF grant DMR-9641291 to J.F.

28 October 1997; accepted 20 February 1998

Friction Anisotropy and Asymmetry of a Compliant Monolayer Induced by a Small Molecular Tilt

M. Liley,* D. Gourdon, D. Stamou, U. Meseth, T. M. Fischer, C. Lutz, H. Stahlberg,† H. Vogel, N. A. Burnham, C. Duschl‡

Lateral force microscopy in the wearless regime was used to study the friction behavior of a lipid monolayer on mica. In the monolayer, condensed domains with long-range orientational order of the lipid molecules were present. The domains revealed unexpectedly strong friction anisotropies and non-negligible friction asymmetries. The angular dependency of these effects correlated well with the tilt direction of the alkyl chains of the monolayer, as determined by electron diffraction and Brewster angle microscopy. The molecular tilt causing these frictional effects was less than 15 degrees, demonstrating that even small molecular tilts can make a major contribution to friction.

Although the nature of friction has been debated since da Vinci's time, a fundamental understanding of friction phenomena has remained elusive. Amontons formulated his law relating friction and the normal load 300 years ago; a hundred years later, Coulomb interpreted friction in terms of cobblestones in a rough road—the bigger the stones, the higher the friction (1). In this century, friction has come to be construed as the plastic degradation of interlocking asperities (2), or to be related to adhesion hysteresis (3). The effect of crystallographic direction on friction was first demonstrated on mica with the surface forces apparatus (4) and later on an organic bilayer with lateral force microscopy (LFM) (5). Recent results, obtained exclusively by LFM, indicated that molecular orientation may also influence friction (6, 7), but no independent structural data were available. Here, we correlated friction data with the molecular orientation as established

by independent methods.

A monolayer of a chiral lipid (8) at the air-water interface was compressed to the coexistence regime where condensed domains form in a fluid matrix (9). This monolayer was transferred to a mica substrate so that the lipids were oriented with the polar head groups toward the mica surface and the alkyl chains exposed to the air (10). LFM (11) on the monolayer revealed flower-like condensed domains. In the lateral force images of the domains (Fig. 1, A and B), each petal of the flower has a different amount of lateral force, whereas the corresponding topography images (not shown here) display no contrast between the different petals (12). For flat samples such as these, the lateral force is equivalent to the tip-sample friction. In the domain shown, there are six major petals and two minor petals. The major petals all have equivalent molecular organization. The minor petals are the result of rotational twinning; they have the same molecular organization as the adjacent major petal, but rotated through 180° (13).

Upon rotation of the sample underneath the microscope tip (Fig. 1B), the friction force on the petals changes in a systematic way. These changes were analyzed using "friction loops" (Fig. 1C), where each loop corresponds to one scan line of the image. The friction force amplitudes L and R for the two scan directions yield the "total friction" $L + R$ and the "friction asymmetry" $L - R$ (14). The variations of the amplitudes L and R correspond to $\sim 25\%$ of the overall friction force.

The total friction and the friction asymmetry were analyzed as a function of the subdomain's angular orientation θ with respect to the scan direction (Fig. 1A); the results of this analysis are shown in Fig. 1, D and E. For both the major and minor subdomains, the total friction has C_2 symmetry (180° periodicity) and the friction asymmetry has C_1 symmetry (360° periodicity). In other words, the friction is not only anisotropic—dependent on the angle of the tip's motion with respect to the domain orientation—but is also asymmetric, that is, different for the trace and retrace of the force microscope tip over the same scan line. There are also differences between the major petals (filled circles) and minor petals (open circles). The two total friction curves are displaced by 30° , a difference that is caused entirely by our definition of the angular direction of the petals. The two friction asymmetry curves are offset by 150° to 210° , which confirms the 180° rotation of molecular organization between major and minor arms.

As a refinement of our analysis, we used the fits of the total friction ($L + R$) and friction asymmetry ($L - R$) to produce simulated lateral force data and images, which we compared with the experimental images. Total friction minus friction asymmetry gave the friction values, R , for the right-to-left scans as a function of angle. These friction values defined the gray levels for the different petals in the simulated images. The success of this simulation of the experimental data (compare Figs. 1B and 1F) allowed us to fix with some certainty the phase angles and relative magnitudes of the fit curves. We conclude that maximum total friction and zero friction asymmetry occurred at 30° , and that the two effects had an amplitude ratio of 10:1.

These friction results led us to investigate the structure of the lipid monolayers. Electron diffraction (Fig. 2A) revealed a hexagonal packing of the alkyl chains (15), with the nearest neighbor directions approximately parallel to the edges of the domain boundaries. The tilt angle of the alkyl chains (to the normal) was estimated to be less than 15° from the normal.

We used Brewster angle microscopy (16) to obtain essential information about the tilt angle of the alkyl chains and their tilt direction (azimuthal angle); this technique is based on the reflection of p-polarized light and allows local determination of these parameters. Experimental images were compared with images (Fig. 2B) calculated using well-established parameters for lipid monolayers (17). The best agreement was obtained for a tilt angle of the alkyl chains of $10^\circ \pm 5^\circ$. The tilt direction was found to lie parallel to the subdomain boundary, as indi-

M. Liley, D. Stamou, U. Meseth, H. Vogel, C. Duschl, Department of Chemistry, Swiss Federal Institute of Technology, CH-1015 Lausanne, Switzerland.

D. Gourdon and N. A. Burnham, Department of Physics, Swiss Federal Institute of Technology, CH-1015 Lausanne, Switzerland.

T. M. Fischer and C. Lutz, Department of Physics, University of Leipzig, Linnestraße 5, D-04103 Leipzig, Germany.

H. Stahlberg, Department of Chemistry, Swiss Federal Institute of Technology, CH-1015 Lausanne, Switzerland, and Department of Biology, University of Lausanne, CH-1015 Lausanne, Switzerland.

*Present address: Centre Suisse d'Electronique et Microtechnique SA, CH-2007 Neuchâtel, Switzerland.

†Present address: Biocenter, University of Basel, CH-4056 Basel, Switzerland.

‡To whom correspondence should be addressed. E-mail: duschl@igcsun3.epfl.ch

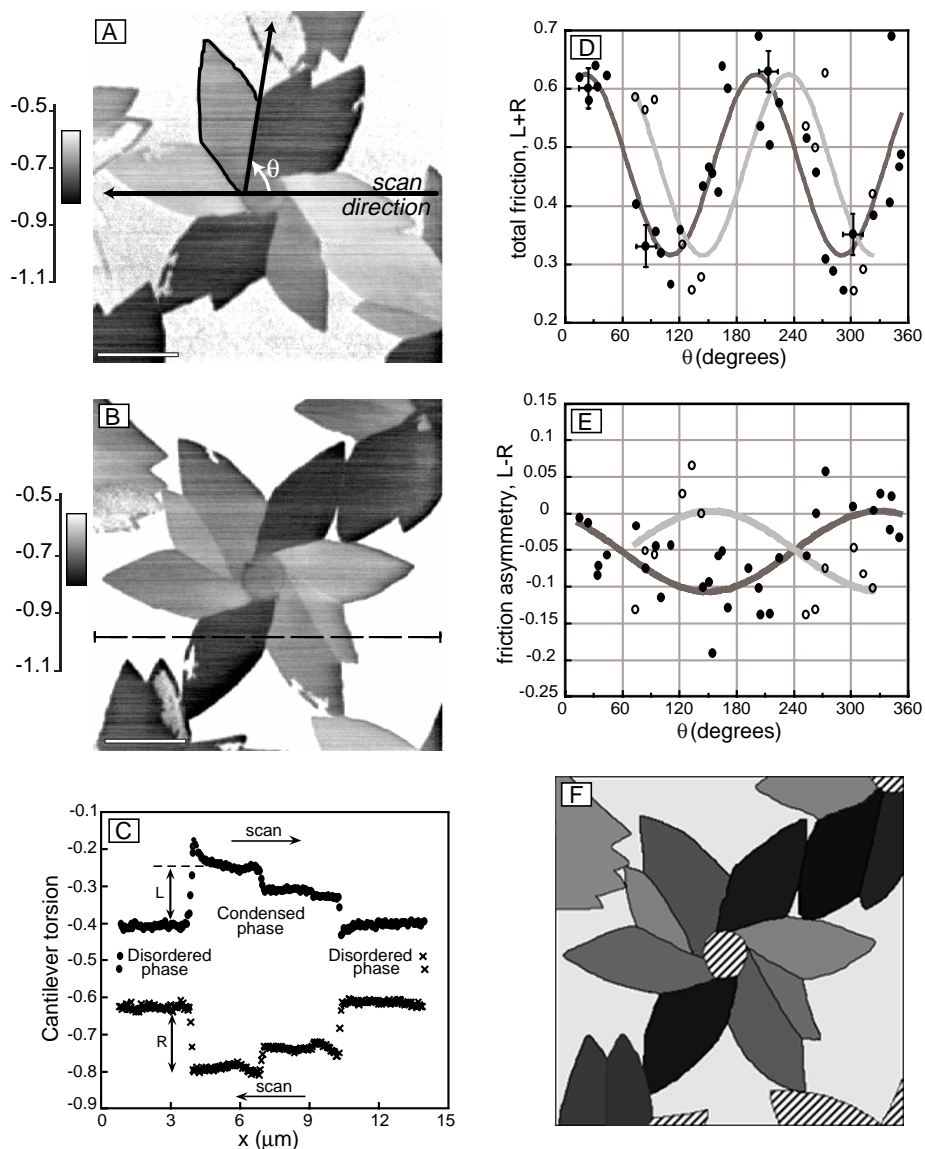


Fig. 1. (A) LFM image of a thiolipid monolayer on a mica surface. A flower-shaped condensed domain can be seen against the disordered phase. The internal structure of the domain is revealed by high friction contrast between the different petals. The angle θ between the lower right petal boundary and the scan direction defines the orientation of the outlined petal. High lateral forces correspond to dark shades of gray. Scale bar, 4 μm ; scan velocity, 42 $\mu\text{m s}^{-1}$. (B) As for (A), after counterclockwise rotation of the sample by 70°. The dashed line is the scan line of the friction loop in (C). (C) A typical friction loop (arbitrary torsion units). The upper curve represents a scan from left to right, the lower curve from right to left. The friction force amplitudes L and R on the condensed domain were defined relative to the disordered phase and were typically 1 to 2 nN. For measurements of the friction forces on the individual petals, 15 adjacent friction loops were averaged. Values of L and R yield the total friction $L + R$ and the friction asymmetry $L - R$. The overshoots seen in some regions of the curve are an artifact caused by the height difference of 1.5 nm between the domains and the matrix. (D) Total friction ($L + R$) versus the orientation of the major petals (filled circles) and minor petals (open circles) with respect to the scan direction as defined in (A). The fit for the major petals (dark line) was based on a sinusoidal curve with a periodicity of 180°; all other parameters were unconstrained. In the fit for the minor petals, the only free parameter was the phase angle. All other parameters were taken directly from the major petal fit. The phase shift between the curves reflects the definition of θ : Relative to the major petals, the subdomain boundaries of the minor petals are displaced by 30°. (E) Friction asymmetry ($L - R$) versus the orientation of the major and minor petals, as in (D). Here, the difference in phase for the major and minor subdomains is between 150° and 210°. (F) A simulated friction force image. The phase angle of ($L + R$) was chosen to give the first maximum at 30°; the phase angle of ($L - R$) was chosen to give zero asymmetry at 30° and 210°. The ratio of the amplitudes of total friction and friction asymmetry is 10:1. These parameters give good agreement between the simulated images and experimental images; compare with the corresponding experimental image (B). Opposing pairs of petals that are oriented roughly perpendicularly to the horizontal scan direction are very similar in their gray levels, whereas pairs of petals directed approximately horizontally have a discernible difference in gray level.

cated by the arrows in Fig. 2B (inset).

We interpret the above structural and friction force results as follows (Fig. 3): The alkyl chains are hexagonally packed and slightly tilted with a uniform tilt direction within each petal. The friction behaves with 180° and 360° periodicity. This implies that the source of the friction anisotropy and asymmetry is the tilt of the alkyl chains within each domain. The maximum total friction is achieved when sliding across the tilt direction (nap); the maximum asymmetry occurs for motion of the tip parallel to the nap. Surprisingly, the friction against the nap of the molecules is lower than with the nap. It is as if stroking a cat tail-to-head were easier than stroking it head-to-tail. This counterintuitive result emphasizes the importance of structural analysis in nanotribology. Only an independent determination of molecular organization allows friction data to be interpreted with certainty.

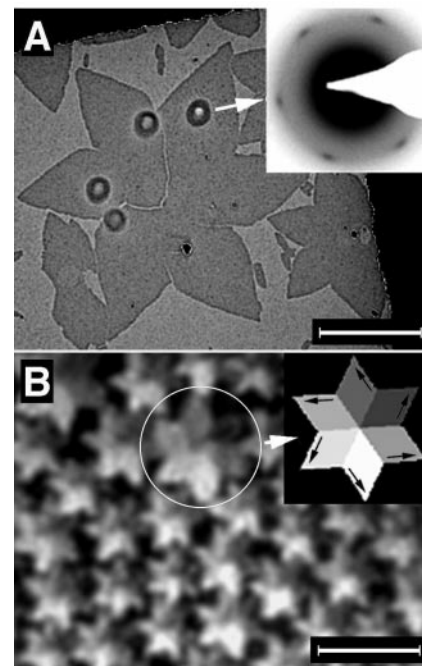


Fig. 2. (A) Electron microscopy image of a monolayer domain. The inset shows the electron diffraction pattern from the spot indicated by the arrow. The diffraction pattern revealed hexagonal packing of the alkyl chains, with the nearest neighbor directions approximately parallel to the subdomain boundaries. A tilt of the alkyl chains should result in a distortion of the diffraction patterns. Because the observed distortion was minimal, the tilt angle is less than 15° to the normal. Scale bar, 8 μm . (B) Brewster angle microscopy image of a thiolipid monolayer at the water-air interface (21). The reflectivity pattern results from the optical anisotropy of the subdomains. The inset, which refers to the encircled domain, shows a simulation of reflectivity based on the Fresnel equations. The tilt direction of the alkyl chains was as indicated by the dark arrows ($\pm 15^\circ$), with a tilt angle to the normal of $10^\circ \pm 5^\circ$. Scale bar, 50 μm .

Earlier work, based only on LFM, wrongly assigned the tilt direction (7).

What could explain the observed friction anisotropy? Traditional interpretations can be ruled out: Asperity interactions, plastic degradation, and adhesion hysteresis fail to account for it. We have found only one other system with behavior analogous to our anisotropy data: anisotropic viscosity in liquid crystals. Liquid crystals consist of rod-like molecules with a preferred orientation, and thus they bear certain similarities to the alkyl chains of our lipid monolayer (18). A few studies on the viscosities of nematic phases of liquid crystals have been published, and they report a consistent pattern of anisotropy: The coefficients of viscosity for flow perpendicular to the rod axis ("director") are higher than those for flow parallel to the director (19). This corresponds well with our measurements; we observed higher total friction (that is, energy dissipation) perpendicular to the tilt direction than parallel to the tilt direction.

We have as yet no explanation for the observed friction asymmetry. Why should there be less friction when scanning against the tilt direction than when scanning with it? We can only note that the energy dissipation is a collective property of the monolayer film and that it should depend (among other things) on the contact area between tip and surface and the tip penetration depth into the film. Perhaps a greater stiffness against the tilt direction reduces the penetration depth and thus the friction forces (20). More experimental and theoretical work on the viscoelastic properties of monolayers will be needed before we can understand the friction behavior observed in this study.

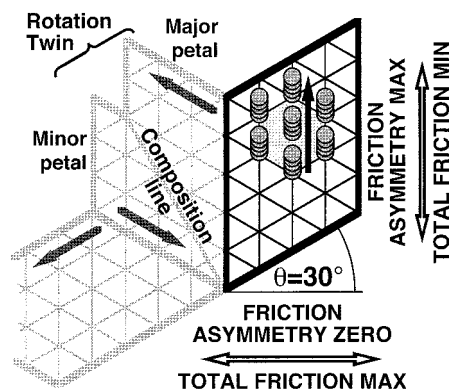


Fig. 3. Correlation of the friction force results (friction directions refer to the black petal) with the results obtained from structural analysis. The grid indicates the lattice directions of the subdomains as revealed by electron diffraction. Filled arrows represent the tilt direction of the alkyl chains as deduced from Brewster angle microscopy. The tilt direction of the minor petal is deduced from the $\sim 180^\circ$ phase difference of the friction asymmetry.

REFERENCES AND NOTES

1. D. Dowson, *History of Tribology* (Longman, London, 1979).
2. F. P. D. Bowden and D. Tabor, *Friction and Lubrication of Solids, Part I* (Oxford Univ. Press, Oxford, 1954).
3. H. Yoshizawa, Y.-L. Chen, J. Israelachvili, *J. Phys. Chem.* **97**, 4128 (1993).
4. M. Hirano, K. Shinjo, R. Kaneko, Y. Murata, *Phys. Rev. Lett.* **67**, 2642 (1991).
5. R. Overney, M. Fujihira, H. Takano, W. Paulus, H. Ringsdorf, *ibid.* **72**, 3546 (1994).
6. L. Santesson *et al.*, *J. Phys. Chem.* **99**, 1038 (1995).
7. D. Gourdon *et al.*, *Tribol. Lett.* **3**, 317 (1997).
8. We used the amphiphile bis[β -(1,2-dipalmitoyl-sn-glycero-3-phosphoryl)-3,6-dioxaoctyl] disulfide ("thio-lipid"), each molecule of which consists of two chiral phospholipids linked by a hydrophilic spacer.
9. H. Lang, C. Duschl, H. Vogel, *Langmuir* **10**, 197 (1994).
10. A. Ulman, *An Introduction to Ultrathin Organic Films: From Langmuir-Blodgett to Self-Assembly* (Academic Press, San Diego, CA, 1991).
11. Lateral force measurements based on optical lever detection were performed under ambient conditions on an M5 atomic force microscope (Park Scientific Instruments). We used V-shaped cantilevers (thickness, $\sim 0.6 \mu\text{m}$) with sharpened conical pure silicon tips and nominal normal and torsional spring constants of 0.03 and 1.2 N m^{-1} , respectively. The tip had a radius of curvature of 40 nm and an amorphous silicon oxide surface. The applied load and the adhesive force were each $\sim 5 \text{ nN}$.
12. The friction contrast is independent of the mica substrate. Similar results were obtained on silicon wafers with amorphous SiO_2 adlayers.
13. C. Giacovazzo, Ed., *Fundamentals of Crystallography* (Oxford Univ. Press, Oxford, 1992), p. 83.
14. U. D. Schwarz, H. Bluhm, H. Hölscher, W. Allers, R. Wiesendanger, in *The Physics of Sliding Friction*, B. N. J. Persson and E. Tosatti, Eds. (Kluwer Academic, Dordrecht, Netherlands, 1996), pp. 369–402.
15. A. Fischer and E. Sackmann, *Nature* **313**, 299 (1985).
16. D. Hörnig and D. Möbius, *J. Phys. Chem.* **95**, 4590 (1991).
17. C. Lautz, J. Kildae, T. M. Fischer, *J. Chem. Phys.* **106**, 7448 (1997).
18. We estimate that the tip penetrates $\sim 5 \text{ \AA}$ into the lipid monolayer domains, which have a thickness of 25 \AA .
19. S. Chandrasekhar, *Liquid Crystals* (Cambridge Univ. Press, Cambridge, 1992).
20. R. M. Overney *et al.*, *Langmuir* **10**, 1281 (1994).
21. Brewster angle microscopy could not be used to characterize the lipid layers on mica because it is an unsuitable substrate for optical reflection techniques.
22. Supported by the Swiss National Research Foundation (NFP 36: 4036-044084/1), SPP Biotechnology, and the board of the Swiss Federal Institutes of Technology (SPP MINAST, 7.06).

17 November 1997; accepted 17 February 1998

Generation of Intestinal T Cells from Progenitors Residing in Gut Cryptopatches

Hisashi Saito, Yutaka Kanamori, Toshitada Takemori, Hideo Nariuchi, Eiro Kubota, Hiromi Takahashi-Iwanaga, Toshihiko Iwanaga, Hiromichi Ishikawa*

Cryptopatches (CPs) are part of the murine intestinal immune compartment. Cells isolated from CPs of the small intestine that were c-kit positive (c-kit⁺) but lineage markers negative (Lin⁻) gave rise to T cell receptor (TCR) $\alpha\beta$ and TCR $\gamma\delta$ intestinal intraepithelial T cells after in vivo transfer or tissue engraftment into severe combined immunodeficient mice. In contrast, cells from Peyer's patches and mesenteric lymph nodes, which belong in the same intestinal immune compartment but lack c-kit⁺Lin⁻ cells, failed to do so. These findings and results of electron microscopic analysis provide evidence of a local intestinal T cell precursor that develops in the CPs.

The gastrointestinal mucosa is one of the largest interfaces in the body with only a single layer of epithelium separating the

exposed external lumen from the internal milieu, and in primitive vertebrates, only gut-associated lymphoid tissues are present (1). Therefore, from an evolutionary perspective, it is possible that the intestinal tract of higher vertebrates retains some self-supporting immune system to ensure internal integrity (2). The numerous intestinal intraepithelial T cells (IELs) have cellular and behavioral characteristics distinct from those of other peripheral T cells (2–6) and are enriched with TCR $\gamma\delta$ T cells (7). In mice, most TCR $\gamma\delta$ IELs and many TCR $\alpha\beta$ IELs, unlike blood-borne T cells, use the CD8 $\alpha\alpha$ homodimer (2, 8) instead of CD8 $\alpha\beta$ and develop somewhere in the intestinal mucosa without passing through the thymus (2, 4, 8, 9).

H. Saito, Y. Kanamori, H. Ishikawa, Department of Microbiology, Keio University School of Medicine, Tokyo 160, Japan.

T. Takemori, Department of Immunology, National Institute of Infectious Diseases, Tokyo 162, Japan.

H. Nariuchi, Department of Allergology, Institute of Medical Science, University of Tokyo, Tokyo 108, Japan.

E. Kubota, Second Department of Oral and Maxillofacial Surgery, Kanagawa Dental College, Kanagawa 238, Japan.

H. Takahashi-Iwanaga, Department of Anatomy, School of Medicine, Hokkaido University, Sapporo 060, Japan.

T. Iwanaga, Laboratory of Anatomy, Graduate School of Veterinary Medicine, Hokkaido University, Sapporo 060, Japan.

*To whom correspondence should be addressed. E-mail: ishikawa@sun.microb.med.keio.ac.jp